Chemically Radiative Flow of Viscoelastic Fluid over Stretching Cylinder with Convective Condition

Bilal Ashraf, Muhammad* [+]

Department of Mathematics, COMSATS University Islamabad, Park Road, Tarlai Kalan, Islamabad 45550, PAKISTAN

ABSTRACT: *This article investigates the mixed convection flow of viscoelastic liquid because of an extending cylinder. The heat transfer investigation has been completed. Energy equation in attendance of heat, radiations are considered. Convective limit conditions for heat and mass exchange are utilized on the outside of the extending cylinder. Suitable transformations are utilized to decrease the overseeing nonlinear partial differential equations into standard differential equations. The subsequent differential equations alongside the boundary conditions are solved analytically by utilizing the homotopy investigation strategy (HAM) for acquiring the convergent series solutions. The effects of physical parameters on the velocity and temperature fields are investigated. Numerical estimations of local Nusselt numbers are computed and analyzed.*

KEYWORDS: *Mixed convection; Thermal radiation; Convective condition; Viscoelastic fluid Stretching cylinder.*

INTRODUCTION

Heat transfer investigation of boundary layer streams of non-Newtonian liquids overextending surface has increased a lot of significance in the ongoing years on account of its event in designing, fabricating, and mechanical procedures. Such streams showed up in glass fiber and paper creation, material industry, streamlined expulsion of plastic sheets, polymeric industry, and so forth. In a large portion of the investigations, the boundary layer equations over linear, non-linear, and exponentially stretching sheets are considered. The flows due to the stretching cylinder have not been discussed extensively in the literature. *Wang* [1] studied the steady incompressible flow of viscous fluid by a stretching hollow cylinder. *Bachok* and *Ishak* [2] investigated the flow and heat transfer over a stretching cylinder with prescribed surface heat flux. Numerical solutions are developed to analyze the flow problem. It is observed that the surface shear stress and the heat transfer rate at the surface increase when the curvature parameter increases. *Mukhopadhyay* [3] investigated the boundary layer flow and heat transfer over a stretching cylinder with slip and MHD effects. *Vajravelu et al.* [4] examined the effects of transverse curvature and temperature-dependent thermal conductivity in the magnetohydrodynamic axisymmetric flow induced by a non-isothermal stretching cylinder. Heat transfer characteristics have been considered in presence of internal heat generation/ absorption. *Rasekh et al.* [5] obtained the numerical solution for the flow of nanofluid past a stretching circular cylinder with a non-uniform heat source. Boundary layer flow of an Eyring--Powell fluid with variable viscosity over a stretching cylinder is discussed by *Malik et al.* [6]. *Sheikholaslami* [7-9] provided

***** *To whom correspondence should be addressed.*
+ *E-mail*: *bilalashraf_qau@yahoo.com*
1021-9986/2021/5/1683-1692 10/$/6.00

the solutions of nanofluid models in presence of entropy by using analytic and numerical techniques.

Mixed convection flow is quite prevalent in various applications of science and technology. Such types of flows occurred due to both external forcing agents and internal volumetric forces. Mixed convection flow problems appear in processes like solar central receivers exposed to winds, electronic devices cooled by fans, nuclear reactors cooled during an emergency shutdown, etc. Natural convection boundary layer flow on a horizontal elliptical cylinder with constant heat flux and temperature-dependent heat generation is studied by *Cheng* [10]. The numerical solutions of governing non-linear equations are presented by the cubic spline collection method. *Mukhopadhyay* [11] investigated the unsteady mixed convection flow over a stretching plate in presence of slip effects. *Hayat et al.* [12] studied the stagnation point flow of Casson fluid with convective boundary conditions. The problem of mixed convection about an inclined flat plate embedded in a porous medium is performed by *Rashidi et al.* [13]. They have used the differential transform method to analyze the flow problem. Sheikholeslami and *Seyednezhad* [14] studied the natural *convection* in a porous medium in presence of an electric field using CVFEM.

In space technology and process relating to high temperatures, the effects of radiation are of vigorous importance for the design of reliable equipment, nuclear plants, gas turbines, and various propulsion devices or aircraft, missiles, satellites, and space vehicles. *Imtiaz et al.* [15] provided the analytical solution of homogeneous-heterogeneous reactions in MHD radiative flow of second-grade fluid due to a curved stretching surface. Effect of melting and heat generation/absorption on Sisko nanofluid over a stretching surface with nonlinear radiation was studied by *Mabood et al.* [16]. *Ashraf et al* [17] presented the solutions for the MHD flow and heat transfer in mixed convection flow of viscoelastic fluid past a stretching surface in presence of Soret and Dufour effects. Also, heat transfer between a solid boundary and static fluid occurs due to conduction purely. Such problems correspond to boundary conditions through Fourier's law of heat conduction. However, the heat transfer through the solid boundary and moving fluid is because of the effects of both conduction and convection. The boundary condition, in this case, is due to the Fourier law of heat conduction and Newton's law of cooling which is termed as convective boundary condition *Ashraf et al.* [18]. To maintain a healthy building given fresh air ventilation convective boundary conditions have the main role.

The objective of the present study is to investigate the mixed convection flow of viscoelastic fluid over a stretching cylinder with thermal radiation. Thermal convective condition is imposed on the surface. The governing boundary layer equations are reduced into the ordinary differential equations by using suitable transformations. The solutions are obtained by employing the homotopy analysis method [19-23]. The behaviors of velocity, temperature, and Nusselt number have been analyzed in presence of thermal radiation and mixed convection parameters.

Governing problems

We consider the steady incompressible flow of viscoelastic fluid by a stretching cylinder at $r=0$. The flow takes place in the domain $r>0$. Here x-axis is taken along the axis of the cylinder and the r -axis is measured along the radial direction. The thermal radiation effect is considered in the presence of the convective condition. The geometry of the flow problem is as follows.

The governing boundary layer equations for the considered flow problems are:

$$\frac{\partial(ru)}{\partial x}+\frac{\partial(rv)}{\partial r}=0 \tag{1}$$

$$u\frac{\partial u}{\partial x}+v\frac{\partial u}{\partial r}=\nu\left(\frac{\partial^2 u}{\partial r^2}+\frac{1}{r}\frac{\partial u}{\partial r}\right)+ \tag{2}$$

$$\frac{k_0}{\rho}\left(\begin{array}{l} u\frac{\partial^3 u}{\partial r^3}+u\frac{\partial^3 u}{\partial x\partial r^2}-\frac{\partial u}{\partial r}\frac{\partial^2 v}{\partial r^2}+\frac{\partial u}{\partial x}\frac{\partial^2 u}{\partial r^2} \\ +\frac{1}{r}\left(v\frac{\partial^2 u}{\partial r^2}+u\frac{\partial^2 u}{\partial x\partial r}-\frac{\partial v}{\partial r}\frac{\partial u}{\partial r}+\frac{\partial u}{\partial x}\frac{\partial u}{\partial r}\right)\end{array}\right)+g\left(\beta_T(T-T_\infty)\right),$$

$$u\frac{\partial T}{\partial x}+v\frac{\partial T}{\partial r}=\sigma\left(\frac{\partial^2 T}{\partial r^2}+\frac{1}{r}\frac{\partial T}{\partial r}\right)-\frac{1}{\rho c_p}\frac{1}{r}\frac{\partial}{\partial r}(rq_r), \tag{3}$$

subjected to the following boundary conditions

$$u(x,r)=u_w(x)=\frac{u_0 x}{l},\quad v(xmr)=0 \tag{4}$$

$$-k\frac{\partial T}{\partial r}=h(T_f-T),\quad \text{at}\quad r=R$$

$$u(x,r)=0,\ v(x,r)=0,\ T(x,r)=T_\infty\quad \text{when } r->\infty \tag{5}$$

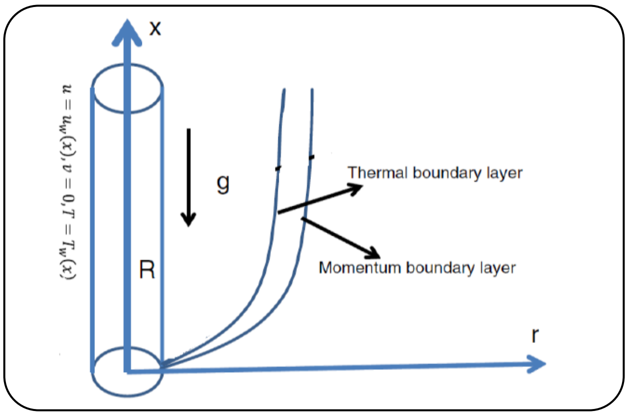

Fig. A: Physical model.

with the surface temperature T_w by

$$T(x,R) = T_w(x) = T_\infty + \left(\frac{x}{l}\right)^n \Delta T \tag{6}$$

In Eqs. (1)-(5) the respective velocity components in the x and r directions are denoted by u and v, k_0 the viscoelastic parameter, k the thermal conductivity, T the fluid temperature, g the gravitational acceleration, β_T the thermal expansion coefficients, σ the thermal diffusivity of fluid, $v = (\mu / \rho)$ the kinematic viscosity, μ the dynamic viscosity of the fluid, ρ the density of the fluid, l the characteristic length, $T_w(x)$ the surface temperature, $u_w(x)$ the stretching velocity, c_p the specific heat, T_∞ the ambient temperature and q_r the radiative heat flux.

The radiative heat flux q_r through Rosseland approximation is

$$q_r = -\frac{4\sigma_s}{3k_e}\frac{\partial T^4}{\partial r} \tag{7}$$

Where σ_s is the Stefan-Boltzmann constant and k_e the mean absorption coefficient. If the temperature differences are sufficiently small then Eq. (7) can be linearized by expanding T^4 into the Taylor series about T_∞ which after neglecting higher-order terms takes the form:

$$T^4 = 4T_\infty^3 T - 3T_\infty^4 \tag{8}$$

By using Eqs. (7) and (8), Eq. (3) reduces to

$$u\frac{\partial T}{\partial x} + v\frac{\partial T}{\partial r} = \sigma\left(\frac{\partial^2 T}{\partial r^2} + \frac{1}{r}\frac{\partial T}{\partial r}\right) + \tag{9}$$

$$\frac{16\sigma_s T_\infty^3}{3k_e \rho c_p}\left(\frac{\partial^2 T}{\partial r^2} + \frac{1}{r}\frac{\partial T}{\partial r}\right)$$

We define the transformations [6]:

$$u = \frac{u_0 x}{l} f'(\eta),\; v = -\frac{R}{r}\sqrt{\frac{u_0 v}{l}} f(\eta), \tag{10}$$

$$\theta(\eta) = \frac{T - T_\infty}{T_f - T_\infty},\; \eta = \sqrt{\frac{u_0}{vl}}\left(\frac{r^2 - R^2}{2R}\right)$$

Now Eq. (1) is automatically satisfied while Eqs. (2, 4), and (9) have the following forms:

$$(1+2\alpha\eta)f''' + 2\alpha f'' + ff'' - f'^2 + 4\alpha K(f'f'' - ff''') + \tag{11}$$

$$K(1+2\alpha\eta)\left(2f'f''' + f''^2 - ff''''\right) + \lambda\theta = 0$$

$$\left(1 + \frac{4}{3}Rd\right)\left((1+2\alpha\eta)\theta'' + 2\alpha\theta'\right) + Pr\left(f\theta' - nf'\theta\right) = 0 \tag{12}$$

$$f = 0,\; f' = 1,\; \theta' = -\gamma\left(1 - \theta(0)\right) \text{ at } \eta = 0 \tag{13}$$

$$f' \leftarrow 0,\; \theta \to 0 \quad \text{as} \quad \eta \to \infty \tag{14}$$

Where α is the curvature parameter, K is the viscoelastic parameter, Pr is the Prandtl number, γ is the Biot number, λ is the local buoyancy parameter, Gr_x is the local Grashof number, Rd is the radiation parameter and prime shows the differentiation with respect to η. These are given by

$$\alpha = \sqrt{\frac{vl}{u_0 R^2}},\quad K = \frac{k_0 u_0}{\rho v l},\quad Pr = \frac{v}{\sigma}, \tag{15}$$

$$\gamma = \frac{h}{k^*}\sqrt{\frac{v}{k}},\quad \lambda = \frac{Gr_x}{Re_x^2},$$

$$Gr_x = \frac{g\beta_T (T_f - T_\infty)x^3}{v^2},\quad R\frac{4\sigma_s T_\infty^3}{3\sigma k_e \rho c_p}$$

Local Nusselt number in dimensionless form is given by

$$Nu/Re_x^{1/2} = -\left(1 + \frac{4}{3}R\right)\theta'(0) \tag{16}$$

in which $Re_x = u_e x / v$ is the local Reynolds number.

Series solutions

The initial approximations and auxiliary linear operators are essential for homotopy analysis solutions. We selected the following initial guesses and auxiliary operators.

$$f_0(\eta) = \left(1 - e^{-\eta}\right),\ \theta_0(\eta) = \frac{\gamma \exp(-\eta)}{1+\gamma} \tag{17}$$

$$L_f = f''' - f',\quad L_\theta = \theta'' - \theta \tag{18}$$

The above auxiliary linear operators satisfy the following properties

$$L_f(C_1 + C_2 e^{\eta} + C_3 e^{-\eta}) = 0, \tag{19}$$
$$L_\theta(C_4 e^{\eta} + C_5 e^{-\eta}) = 0$$

where C_i (i = 1-5) indicates the arbitrary constants.

The corresponding problems at the zeroth order are

$$(1-p)L_f\left[\hat{f}(\eta;p) - f_0(\eta)\right] = p\hbar_f \mathbf{N}_f\left[\hat{f}(\eta;p), \hat{\theta}(\eta,p)\right] \tag{20}$$

$$(1-p)L_\theta\left[\hat{\theta}(\eta;p) - \theta_0(\eta)\right] = \tag{21}$$
$$p\hbar_\theta \mathbf{N}_\theta\left[\hat{f}(\eta;p), \hat{\theta}(\eta,p)\right]$$

$$\hat{f}(0;p) = 0,\ \hat{f}'(0;p) = 1,\ \hat{f}'(\infty;p) = 0 \tag{22}$$
$$\hat{\theta}'(0,p) = -\gamma[1 - \theta(0,p)],\ \hat{\theta}(\infty,p) = 0,$$

$$\mathbf{N}_f[\hat{f}(\eta,p), \hat{\theta}(\eta,p)] = (1 + 2\alpha\eta)\frac{\partial^3 \hat{f}(\eta,p)}{\partial\eta^3} + \tag{23}$$
$$2\alpha\frac{\partial^2 \hat{f}(\eta,p)}{\partial\eta^2} + \frac{\partial \hat{f}(\eta,p)}{\partial\eta}\frac{\partial^2 \hat{f}(\eta,p)}{\partial\eta^2}$$
$$-\left(\frac{\partial \hat{f}(\eta,p)}{\partial\eta}\right)^2 + 4\alpha K\begin{pmatrix}\frac{\partial \hat{f}(\eta,p)}{\partial\eta}\frac{\partial^2 \hat{f}(\eta,p)}{\partial\eta^2} \\ -\hat{f}(\eta,p)\frac{\partial^3 \hat{f}(\eta,p)}{\partial\eta^3}\end{pmatrix}$$
$$+K(1 + 2\alpha\eta)\begin{pmatrix}2\frac{\partial \hat{f}(\eta,p)}{\partial\eta}\frac{\partial^3 \hat{f}(\eta,p)}{\partial\eta^3} + \\ \left(\frac{\partial^2 \hat{f}(\eta,p)}{\partial\eta^2}\right)^2 - \hat{f}(\eta,p)\frac{\partial^4 \hat{f}(\eta,p)}{\partial\eta^4}\end{pmatrix} + \lambda\hat{\theta}(\eta,p)$$

$$N_\theta\left[\hat{\theta}(\eta,p),\ \hat{f}(\eta,p)\right] = \tag{24}$$
$$\left(1 + \frac{4}{3}R\right)\begin{pmatrix}(1 + 2\alpha\eta)\frac{\partial^2 \hat{\theta}(\eta,p)}{\partial^2\eta^2} \\ +2\alpha\frac{\partial^2 \hat{\theta}(\eta,p)}{\partial\eta}\end{pmatrix} + pr\begin{pmatrix}\hat{f}(\eta,p)\frac{\partial^2 \hat{\theta}(\eta,p)}{\partial\eta} \\ -n\hat{\theta}(\eta,p)\frac{\partial^2 \hat{f}(\eta,p)}{\partial\eta}\end{pmatrix}$$

Here p is an embedding parameter, $\hbar_f$ and $\hbar_\theta$ are the non-zero auxiliary parameters. $\mathbf{N}_f$ and $\mathbf{N}_\theta$ indicate the nonlinear operators. When $p=0$ and p = 1 one has:

$$\hat{f}(\eta;0) = f_0(\eta),\ \hat{\theta}(\eta,0) = \theta_0(\eta), \tag{25}$$
$$\hat{f}(\eta;1) = f(\eta),\ \hat{\theta}(\eta,1) = \theta(\eta)$$

Clearly when p is increased from 0 to 1 then f (η,p) and θ(η,p) vary from $f_0(\eta)$ and $\theta_0(\eta,p)$ to f(η) and θ(η). By Taylor's expansion we have

$$f(\eta,p) = f_0(\eta) + \sum_{m=1}^{\infty} f_m(\eta)p^m, \tag{26}$$
$$f_m(\eta) = \frac{1}{m!}\left.\frac{\partial^m f(\eta;p)}{\partial\eta^m}\right|_{p=0},$$

$$\theta(\eta,p) = \theta_0(\eta)\sum_{m=1}^{\infty} \theta_m(\eta)p^m, \tag{27}$$
$$\theta_m(\eta) = \frac{1}{m!}\left.\frac{\partial^m \theta(\eta;p)}{\partial\eta^m}\right|_{p=0}$$

The convergence of the above series strongly depends upon $\hbar_f$ and $\hbar_\theta$. Considering that $\hbar_f$ and $\hbar_\theta$ are selected properly so that Eqs. (26) and (27) converge at p = 1 then we can write

$$f(\eta) = f_0(\eta) + \sum_{m=1}^{\infty} f_m(\eta), \tag{28}$$

$$\theta(\eta) = \theta_0(\eta) + \sum_{m=1}^{\infty} \theta_m(\eta) \tag{29}$$

The resulting problems at mth order deformation can be constructed as follows:

$$L_f[f_m(\eta) - \chi_m f_{m-1}(\eta)] = \hbar_f \mathbf{R}_f^m(\eta), \tag{30}$$

$$L_\theta[\theta_m(\eta) - \chi_m \theta_{m-1}(\eta)] = \hbar_\theta \mathbf{R}_\theta^m(\eta) \tag{31}$$

$$f_m(0) = f_m'(0) = f_m'(\infty) = 0, \tag{32}$$
$$\theta_m'(0) - \gamma\theta_m(0) = \theta_m(\infty) = 0$$

$$\mathbf{R}_f^m(\eta) = (1 + 2\alpha\eta)f_{m-1}'''(\eta) + 2\alpha f_{m-1}''(\eta) + \tag{33}$$
$$\sum_{k=0}^{m-1} f_{m-1-k}f_k'' - \sum_{k=0}^{m-1} f_{m-1-k}'f_k' + 4\alpha K\sum_{k=0}^{m-1}\begin{pmatrix}f_{m-1-k}'f_k'' \\ -f_{m-1-k}f_k'''\end{pmatrix} +$$
$$K(1 + 2\alpha\eta)\begin{pmatrix}2\sum_{k=0}^{m-1} f_{m-1-k}'f_k''' + \\ \sum_{k=0}^{m-1} f_{m-1-k}''f_k'' - \sum_{k=0}^{m-1} f_{m-1-k}f_k''''\end{pmatrix}$$

$$R^{m}_{\theta}(\eta) = \left(1+\frac{4}{3}R\right)\left((1+2\alpha\eta)\theta''_{m-1}(\eta)+2\alpha\theta'_{m-1}(\eta)\right)+ \Pr\sum_{k=0}^{m-1}\begin{pmatrix}\theta'_{m-1-k}f_k\\ -nf''_{m-1-k}\theta_k\end{pmatrix} \quad (34)$$

Solving the above mth order deformation problems we have

$$f_m(\eta) = f^{*}_m(\eta) + C_1 + C_2e^{\eta} + C_3e^{-\eta} \quad (35)$$

$$\theta_m(\eta) = \theta^{*}_m(\eta) + C_4e^{\eta} + C_5e^{-\eta} \quad (36)$$

in which the f^{*}_m and θ^{*}_m indicate the special solutions.

Convergence analysis and discussion

The auxiliary parameters $\hbar_f$ and $\hbar_\theta$ are involved in the series solutions Eq. (35) and Eq. (36). These parameters have a pivotal role in controlling the convergence of homotopic solutions. For obtaining the suitable ranges $\hbar_f$ and $\hbar_\theta$ the $\hbar-$ curves are displayed in the 15th order of approximations. The acceptable values of $\hbar_f$ and $\hbar_\theta$ are $-1.4 \le \hbar_f \le -0.30$ and $-1.60 \le \hbar_\theta \le -0.25$ (see Fig.1). Table 1 ensures that the developed series solutions converge in the whole region of η when $\hbar_f = \hbar_\theta = -0.7$.

Figs. 2a-2e are drawn to see the impacts of curvature parameter α, viscoelastic parameter K, mixed convection parameter λ Biot number γ and temperature exponent n on the velocity profile $f'(\eta)$. Fig. 2a depicts the influence of curvature parameter α on the velocity profile $f'(\eta)$. It is noted that both the momentum boundary layer thickness and the velocity profile $f'(\eta)$ increase when we increase the values of the curvature parameter α. This is due to the fact that when we increase the curvature parameter α, the radius of the cylinder decreases so the area of the cylinder in contact with fluid decreases. The effect of viscoelastic parameter K on the velocity profile $f'(\eta)$ is analyzed in Fig. 2b. As expected both the velocity profile $f'(\eta)$ and momentum boundary layer thickness are increasing functions of viscoelastic parameter K. In fact viscoelastic parameter is inversely proportional to the viscosity of the fluid. Higher values of K correspond to a reduction in viscosity. Such reduction in viscosity enhances the fluid velocity.

***Table 1**: Convergence of series solutions for different order of approximations when α = K= 0.2, R= n = 0.3, Pr = 1.0, λ = 0.5, γ = 0.4 and $\hbar_f = \hbar_\theta = -0.7$.*

order of approximations	-f" (0)	-θ (0)
1	0.65289	0.27124
5	0.65936	0.26148
10	0.65776	0.26110
15	0.65760	0.26113
20	0.65755	0.26114
25	0.65753	0.26114
30	0.65753	0.26114

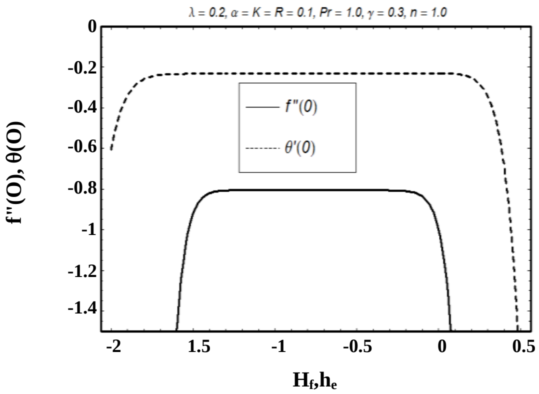

***Fig. 1:** ħ- curves for the functions f(η) and θ(η).*

From Fig. 2c we examined that the momentum boundary layer thickness and velocity field $f'(\eta)$ increase with an increase in λ. Physically an increase in λ implies the addition of buoyancy-induced flow onto the external flow and thus the velocity increases. Variation of Biot number γ on the velocity profile $f'(\eta)$ is analyzed in Fig. 2d. It is observed that the velocity profile $f'(\eta)$ increases when there is an increase in γ. Fig. 2e is drawn to see the impact of temperature exponent n on the velocity field $f'(\eta)$. It is exposed that both the momentum boundary layer thickness and the velocity field $f'(\eta)$ decrease for higher values of n.

Figs. 3a-3g are sketched to examine the influence of curvature parameter α, the viscoelastic parameter K, mixed convection parameter λ, Biot number γ, radiation parameter R, Prandtl number Pr and temperature exponent n on the temperature profile $\theta(\eta)$. Fig. 3a shows that

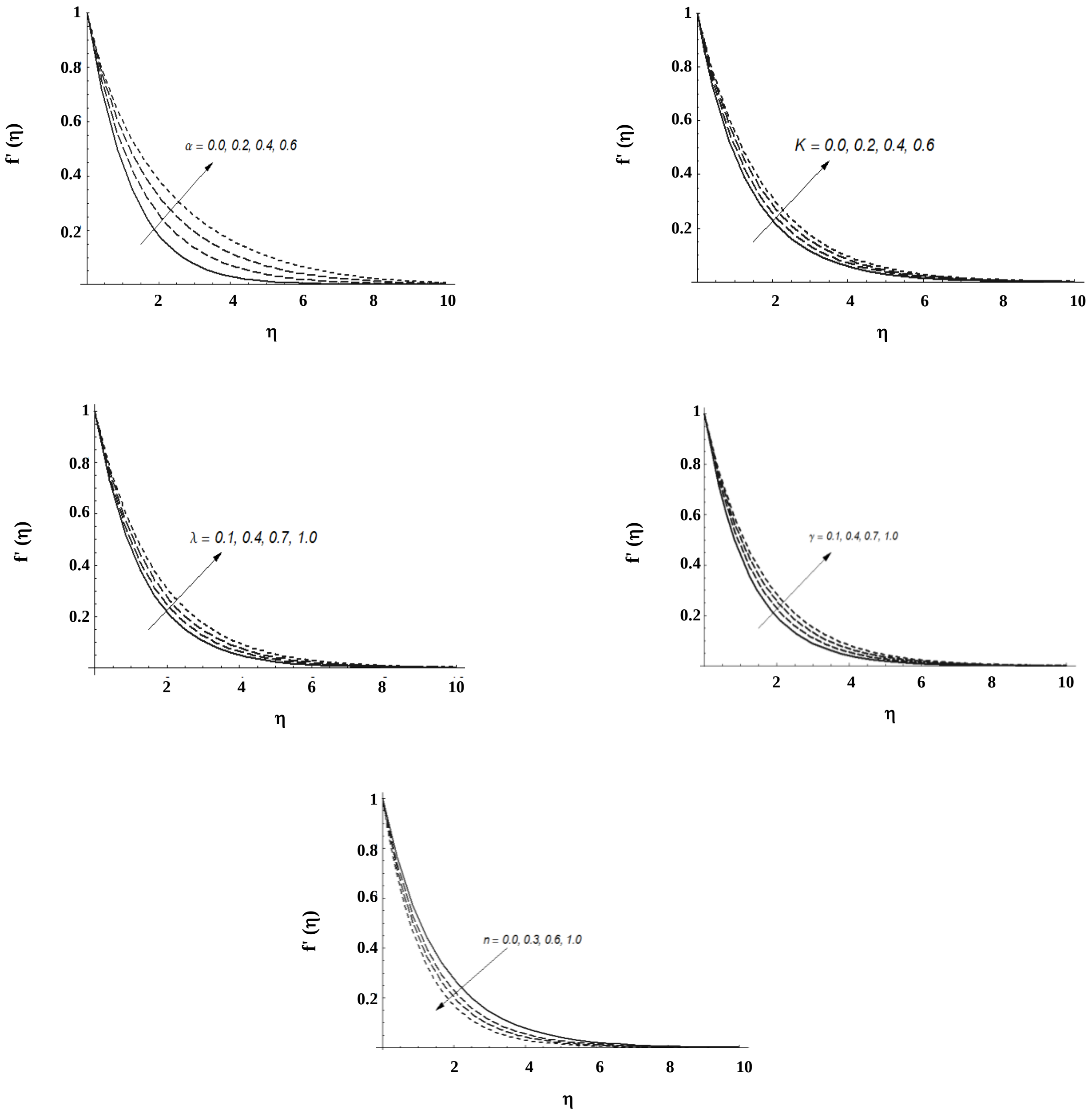

Fig. 2: a) Influence of α on the velocity $f'(\eta)$ when K = 0.2, γ = 0.4, λ = 0.5, R = 0.3, n = 1.0 and Pr = 0.7. b) Influence of K on the velocity $f'(\eta)$ when α = 0.2, γ = 0.4, λ = 0.5, R = 0.3, n = 1.0 and Pr = 0.7. c) Influence of λ on the velocity $f'(\eta)$ when α = 0.2, γ = 0.4, K = 0.5, R = 0.3, n = 1.0 and Pr = 0.7. d) Influence of γ on the velocity $f'(\eta)$ when α = 0.2, λ = 0.5, K = 0.5, R = 0.3, n = 1.0 and Pr = 0.7. e) Influence of n on the velocity $f'(\eta)$ when α = 0.2, λ = 0.5, K = 0.5, R = 0.5, n = 1.0 and Pr = 0.7.

temperature field $\theta(\eta)$ decreases near the wall while it increases far away from the wall as the curvature parameter α increases. This is due to the fact that within the increase of α the particles near the wall loses friction between the particles. Fig. 3b elucidates that an increase in viscoelastic parameter K decreases the temperature and thermal boundary layer thickness. Fig. 3c is displayed to see the influence of mixed convection parameter λ on the temperature $\theta(\eta)$. It is noted from Fig. that the temperature $\theta(\eta)$ is decreasing function of λ. Further, we observed that the thermal boundary layer thickness also decreases for larger λ. Variation of Biot number γ

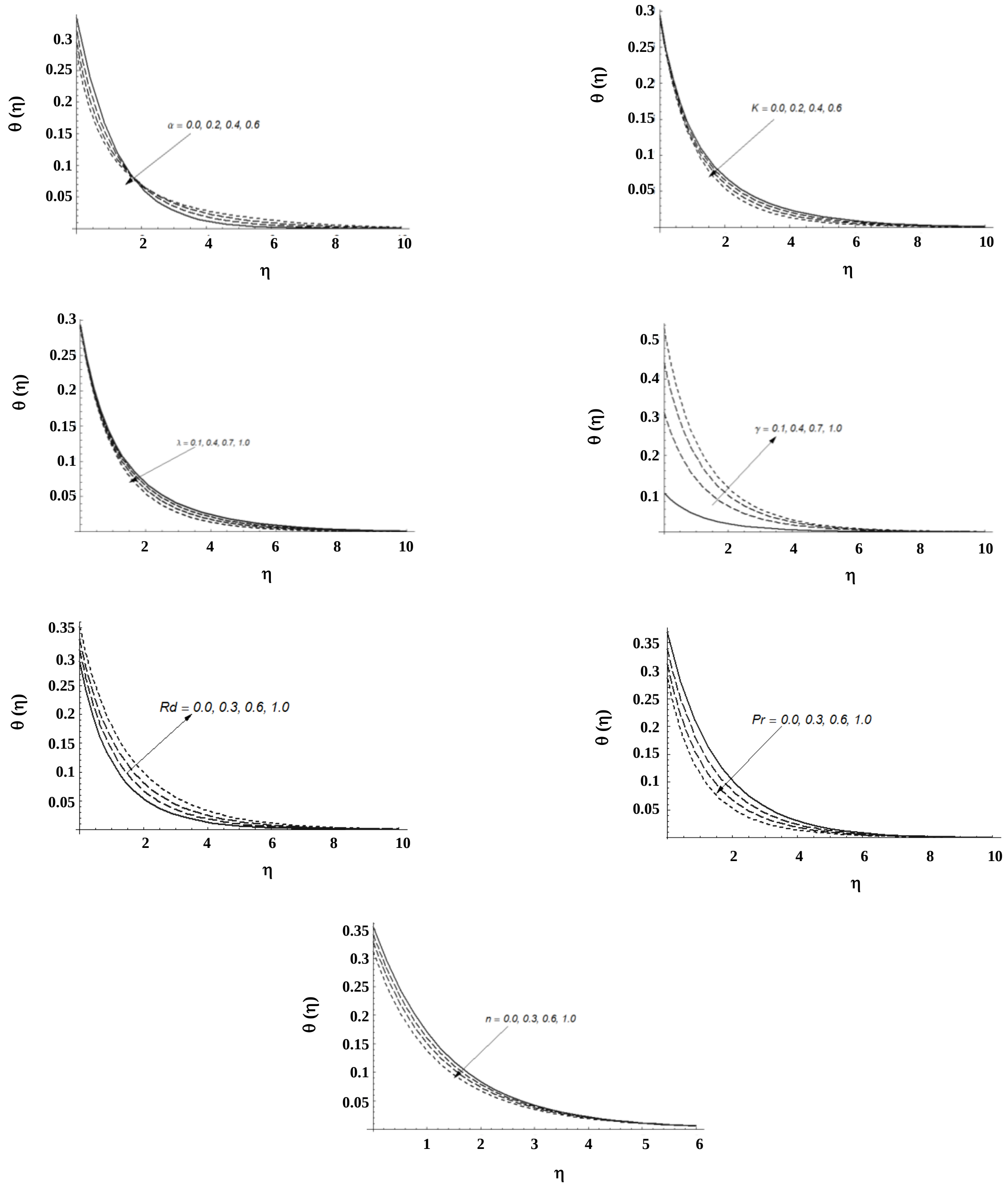

Fig. 3: a) Influence of α on the temperature $\theta(\eta)$ when K = 0.2, γ = 0.4, λ = 0.5, R = 0.3, n = 1.0 and Pr = 0.7. b) Influence of K on the temperature $\theta(\eta)$ when α = 0.2, γ = 0.4, λ = 0.5, R = 0.3, n = 1.0 and Pr = 0.7. c) Influence of λ on the temperature $\theta(\eta)$ when α = 0.2, γ = 0.4, λ = 0.5, R = 0.3, n = 1.0 and Pr = 0.7. d) Influence of γ on the temperature $\theta(\eta)$ when α = 0.2, λ = 0.4, K = 0.5, R = 0.3, n = 1.0 and Pr = 0.7. e) Influence of Rd on the temperature when K = 0.2, γ = 0.4, λ = 0.5, n = 1.0 and Pr = 0.7. f) Influence of $\Pr$ on the temperature $\theta(\eta)$ when α = 0.2, λ = 0.5, γ = 0.4, K = R = 0.3, and n = 1.0. g) Influence of n on the temperature $\theta(\eta)$ when α = 0.2, λ = 0.5, γ = 0.4, K = R = 0.3 and Pr = 0.7.

Table 2: Values of local Nusselt number $-\left(1+\frac{4}{3}R\right)\theta'(0)$ ***for different values of*** α, β, λ, ***n, R, Pr and*** γ.

α	K	λ	Rd	Pr	γ	n	$-\left(1+\frac{4}{3}R\right)\theta'(0)$
0.0	0.2	0.5	0.3	1.0	0.4	0.3	0.24822
0.2							0.26114
0.3							0.26630
0.2	0.0						0.25928
	0.2						0.26110
	0.4						0.26254
0.2	0.2	0.0					0.25911
		0.3					0.26039
		0.5					0.26114
0.2	0.2	0.5	0.0				0.27381
			0.3				0.26114
			0.5				0.25402
0.2	0.2	0.5	0.3	1.0			0.26114
				1.5			0.28045
				2.0			0.29311
0.2	0.2	0.5	0.3	1.0	0.2		0.15773
					0.5		0.30070
					0.7		0.36385
0.2	0.2	0.5	0.3	1.0	0.4	0.0	0.24362
						0.5	0.27001
						1.0	0.28638

on the temperature $\theta(\eta)$ is seen in Fig. 3d. It is examined that both the temperature $\theta(\eta)$ and thermal boundary layer thickness increase when Biot number γ is increased. This is due to the fact that Biot number γ is the ratio of internal thermal resistance of a solid to the boundary layer thermal resistance. Fig. 3e is drawn to analyze the behavior of radiation parameter R on the temperature profile $\theta(\eta)$. Thermal radiation is electromagnetic radiation generated by the thermal motion of charged particles in matter. All matter with a temperature greater than absolute zero emits thermal radiation. The mechanism is that bodies with a temperature above absolute zero have atoms or molecules with kinetic energies which are changing. These changes result in charge-acceleration and/or dipole oscillation of the charges that compose the atoms. This motion of charges produces electromagnetic radiation in the usual way. However, the wide spectrum of this radiation reflects the wide spectrum of energies and accelerations of the charges in any piece of matter at even a single temperature. That's why it is seen in Fig. 3f that an increase in radiation parameter R gives rise to the thermal boundary layer and temperature. To see the influence of Prandtl number Pr on the temperature field $\theta(\eta)$ Fig. 3f is plotted. It is noticed from this Fig. it is examined that both the thermal boundary layer and temperature $\theta(\eta)$ are decreasing functions of Pr. This is due to the fact that the Prandtl number is the ratio of momentum and thermal diffusivities. An increase in Pr shows lower thermal diffusivity. This change in thermal diffusivity causes a reduction in energy transfer ability and ultimate in the decrease of the thermal boundary layer. Fig. 3g is displayed to explore the impact of temperature exponent n on the temperature $\theta(\eta)$. It is concluded that the effect of n for both the thermal boundary layer and the temperature $\theta(\eta)$ is similar to that of Prandtl number Pr. Table 2 is presented to see the numerical values of the local Nusselt number $-\left(1+\frac{4}{3}R\right)\theta'(0)$.

The values of the local Nusselt number increase with an increase in curvature parameter α, viscoelastic parameter K, mixed convection parameter λ, Prandtl number Pr, Biot number γ and temperature exponent n while it is reduced for higher values of radiation parameter R.

CONCLUSIONS

This article explores the characteristics of viscoelastic fluid in the flow by a stretching cylinder with convective boundary conditions. The problem is investigated in presence of mixed convection and thermal radiation effects. The main points of the presented analysis are:

- Influences of curvature parameter α and fluid model parameter K on the velocity and temperature profiles are quite opposite.
- Effects of mixed convection parameter λ on momentum and thermal boundary layers are reversed.
- Features of γ and n on the velocity and temperature profiles are similar.
- Thermal boundary layer thickness and temperature $\theta(\eta)$ decrease with an increase in Pr and n.
- Local Nusselt number is an increasing function of γ, Pr, n, α, K and λ while it decreases for R.

Received : Apr. 5, 2020 ; Accepted : Jun. 15, 2020

REFERENCES

[1] Wang C.Y., Fluid Flow Due to a Stretching Cylinder, *Phys. Fluids.*, **31**: 466-468 (1988).

[2] Bachok N., Ishak A., Flow and Heat Transfer over a Stretching Cylinder with Prescribed Surface Heat Flux, *Malaysian J. Math. Sci.*, **4**: 159-169 (2010).

[3] Mukhopadhyay S., Slip Effects on Boundary Layer Flow and Heat Transfer Along a Stretching Cylinder, *Int. J. Appl. Mech. Eng.*, **18**: 447-459 (2013).

[4] Vajravelu K., Parsad K.V., Santhi S.R., Axisymmetric Magneto-Hydrodynamic (MHD) Flow and Heat Transfer at a Non- Isothermal Stretching Cylinder, *Appl. Math. Comput.*, **219**: 3993-4005 (2012).

[5] Rasekh A., Ganji D.D., Tavakoli S., Numerical Solutions for a Nanofluid Past over a Stretching Circular Cylinder with Non-Uniform Heat Source, *Front. Heat Mass Transf.*, **3**: 043003 (2012).

[6] Malik M.Y., Hussain A., Nadeem S., Boundary Layer Flow of an Eyring--Powell Model Fluid Due to a Stretching Cylinder with Variable Viscosity, *Scientia Iranica*, **20**: 313-321 (2013).

[7] Sheikholeslami M., New Computational Approach for Exergy and Entropy Analysis of Nanofluid under the Impact of Lorentz Force Through a Porous Media, *Computer Methods in Applied Mechanics and Engineering*, **344**: 319–333 (2019).

[8] Sheikholeslami M., Finite Element Method for PCM Solidification in Existence of CuO Nanoparticles, *Journal of Molecular Liquids*, **265**: 347–355 (2018).

[9] Sheikholeslami M., Rezaeian Jouybari B., Darzi M., Shafee A., Li Z., Nguyen T.K., Application of Nano-Refrigerant for Boiling Heat Transfer Enhancement Employing an Experimental Study, *International Journal of Heat and Mass Transfer*, **141**: 974–980 (2019).

[10] Cheng C.Y., Natural Convection Boundary Layer on a Horizontal Elliptical Cylinder with Constant Heat Flux and Internal Heat Generation, *Int. Commun. Heat Mass Transf.*, **36**: 1025-1029 (2009).

[11] Mukhopadhyay S., Effects of Slip-on Unsteady Mixed Convective Flow and Heat Transfer Past a Stretching Surface, *Chin. Phys. Lett.*, **12**: 124401 (2010).

[12] Hayat T., Shehzad S.A., Alsaedi A., Alhothuali M.S., Mixed Convection Stagnation Point Flow of Casson Fluid with Convective Boundary Conditions, *Chin. Phys. Lett.*, **11**: 114704 (2012).

[13] Rashidi M.M., laraqi N., Sadri S.M., A Novel Analytical Solution of Mixed Convection About an Inclined Flat Plate Embedded in a Porous Medium Using the DTM-Padé, *Int. J. Therm. Sci.*, **49**: 2405-2412 (2010).

[14] Sheikholeslami M., Seyednezhad M., Simulation of Nanofluid Flow and Natural Convection in a Porous Media Under the Influence of Electric Field Using CVFEM, *International Journal of Heat and Mass Transfer*, **120**: 772–781 (2018).

[15] Bilal Ashraf M., Hayat T., Alsulami H., Mixed Convection Falkner-Skan Wedge Flow of an Oldroyd-b Fluid in Presence of Thermal Radiation, *Journal of Applied Fluid Mechanics*, **9**: 1753-1762 (2016).

[16] Mabood F., Ibrahim S. M., Khan W.A., Effect of Melting and Heat Generation/Absorption on Sisko Nanofluid over a Stretching Surface with Nonlinear Radiation, *Physica Scripta*, **94**: 065701 (2019).

[17] Imtiaz M., Mabood F., Hayat T., Alsaedi A., Homogeneous-Heterogeneous Reactions in MHD Radiative Flow of Second Grade Fluid Due to a Curved Stretching Surface., *Int. J. Heat Mass Transfer*, **145**: 118781 (2019).

[18] Bilal Ashraf M., Hayat T., Alsaedi A., Shehzad S.A., Soret and Dufour Effects on the Mixed Convection Flow of an Oldroyd-B Fluid with Convective Boundary Conditions, *Results in Physics*, **6**: 917-924 (2016).

[19] Bilal Ashraf M., Hayat T., Shehzad S.A., Ahmed B., Thermophoresis and MHD Mixed Convection Three-Dimensional Flow of Viscoelastic Fluid with Soret and Dufour Effects, *Neural Computing and Applications*, **31**: 249-261 (2019).

[20] Bilal Ashraf M., Hayat T., Alseadi A., Mixed Convection Flow of Casson Fluid over a Stretching Sheet with Convective Boundary Conditions and Hall Effect, *Boundary Value Problems*, **2017**: 1-17 (2017).

[21] Abbasbandy S., Hashemi M.S., Hashim I., On Convergence of Homotopy Analysis Method and its Application to Fractional Integro-Differential Equations, *Quaestiones Mathematicae*, **36**: 93-105 (2013).

[22] Bilal Ashraf M., Hayat T., Alseadi A., Radiative Mixed Convection Flow of an Oldroyd-B Fluid over an Inclined Stretching Surface, *Journal of Applied Mechanics and Technical Physics*, **57**: 317-325 (2016).

[23] Mabood F., Lorenzini G., Pochai N., Shateyi S., Homotopy Analysis Method for Radiation and Hydrodynamic-Thermal Slips Effects on MHD Flow and Heat Transfer Impinging on Stretching Sheet, *Defect and Diffusion Forum*, **388**: 317-327 (2018).